Paper AIAA 2014-2496 7th AIAA Theoretical Fluid Mechanics Conference, Atlanta GA June 2014

Experimental Investigation of Gas Injection into the Boundary Layer on a Slender Body in Supersonic Flow

B. E. Schmidt*, N. P. Bitter*, H. G. Hornung†, J. E. Shepherd‡
California Institute of Technology, Pasadena, California, 91125, USA

A method for injection of gas into the boundary layer on a slender body in supersonic flow while minimizing perturbation to the mean flow is examined experimentally. Injection of gas is equivalent to a sudden increase in the displacement thickness of the boundary layer, which produces an oblique shock that propagates into the inviscid region of the flow. It is found that modification of the geometry of the body can compensate for the increased displacement thickness created by injection and minimize the production of oblique waves. However, the resulting near-wall injection layer is observed to be unstable and a turbulent boundary layer develops downstream of the injection region. The instability of the flow is examined using velocity profiles from a compressible Navier-Stokes computation. In-depth analysis of the mean flow and stability are performed by Fedorov in a companion paper.

Nomenclature

Re	Reynolds Number
M	Mach Number
γ	Ratio of specific heats
U	Velocity, m/s
p	Pressure, Pa
ρ	Density, kg/m^3
T	Temperature, K
δ	Injection/Boundary Layer thickness
m	Normalized injection mass flow rate
ω	Frequency, rad/s
α	Spatial growth rate, 1/s

Subscript

∞	Freestream quantity
e	Injection/Boundary Layer edge quantity
w	Wall quantity

For porous media flow (Section III)

R	Specific gas constant, J/kg K
$\dot{m}$	Mass flow rate, kg/s
μ	Dynamic viscosity, kg/m s
L	Length of injector, m
κ	Permeability, m^2
r	Injector radius, m
$\bar{d}$	Mean particle diameter, m
ϵ	Porosity

*Graduate Student, Aerospace Engineering, 1200 E California Blvd. MC 205-45, Student Member
†Professor, Aerospace Engineering, 1200 E California Blvd. MC 205-45, Fellow
‡Professor, Aerospace Engineering, 1200 E California Blvd. MC 205-45, Member

I. Introduction

Injection of a gas into the boundary layer in a supersonic flow has a number of applications to high speed flight. In scramjet inlets, injection can reduce skin friction drag, cool the wall by film cooling, increase the resistance of the boundary layer to separation via transition to turbulence, and mix some fuel with air prior to entering the combustor.[1,2] The motivation for the present study is the potential for instability control by the modification of boundary layer gas composition. The concept is based on the observation that gases that are vibrationally active can convert acoustic energy into thermal energy, damping waves associated with boundary layer instability and delaying transition to turbulence.[3] However, injection is also potentially destabilizing because of the modification of the boundary layer velocity profile and the potential for adverse pressure gradients due to oblique shock wave generation.

I.A. Hypervelocity boundary layer transition

Hypervelocity boundary layers are highly unstable to acoustic disturbances via the so-called second or Mack mode.[4] The growth rates for the first mode, caused by Tollmien-Schlichting instability, are much smaller compared to that of the Mack mode when the freestream Mach number is high. The growth rate for the Mack mode is also dependent on the enthalpy of the flow and in high enthalpy flow, corresponding to hypersonic flight, the Mack mode is dominant in controlling boundary layer transition.

Current understanding of the mechanism for the Mack mode is summarized in Fedorov et al.,[5] and the reader is referred here for a more complete discussion. It is an inviscid instability brought about by trapped acoustic waves inside the boundary layer. The velocity and sound speed profiles in the boundary layer create a wave guide that refracts acoustic disturbances towards the wall and prevents them from escaping. The energy carried by this trapped acoustic radiation is amplified and eventually leads to turbulence. The line where the phase speed of the disturbance is equal to the sum of the flow velocity and the local sound speed, called the sonic line, acts as the wave guide.

Past research has shown that acoustic energy can be absorbed by nonequilibrium effects in the gas in the boundary layer.[6,7] This occurs if two conditions are met: energy exchange between vibrational and translational/rotational modes must occur on the same time scale as the period of the most amplified frequency in the boundary layer, and the vibrational energy modes must be sufficiently populated to absorb a significant amount of acoustic energy. Both of these conditions are met for carbon dioxide at high enthalpy flow conditions. The most amplified frequency in hypervelocity boundary layers is on the order of 1 MHz. For these reasons, if carbon dioxide could be injected into the boundary layer in a hypervelocity air flow without creating a significant disturbance, transition to turbulence would be delayed.

I.B. Previous Work

CO_2 injection was previously tested in the T5 hypervelocity shock tunnel at Caltech by Leyva and Jewell.[3,8] These experiments were performed using a porous conical injector made from sintered stainless steel, the slope of which matches the slope of the cone model, shown in Figure 1. One complicating factor in interpreting these experiments is that previous studies have shown that a porous surface with no injection absorbs acoustic energy and can significantly delay or suppress boundary layer transition.[9] The results are inconclusive regarding the effectiveness of injection on delaying the onset of boundary layer transition, motivating a closer study of the effects of gaseous injection in supersonic flow.

Upon further investigation, it is clear that injection from a conical injector creates a disturbance to the mean flow, which is undesirable. The injected gas can be seen as increasing the displacement thickness of the boundary layer over a short distance, which has the effect of a positive angle change of the surface of the cone. This causes an oblique shock to form that propagates into the exterior flow and creates an adverse pressure gradient on the surface, along with another wave system downstream related to the specifics of the injected gas flow.

It was hypothesized by A. Fedorov that a negative slope of the injector section could compensate for the increase in the displacement thickness caused by injection. This would minimize the strength of the oblique shock and other waves if the injection rate was properly tuned. An illustration of this idea is shown in Figure 2. An Euler simulation was carried out to test this hypothesis, and it partially demonstrates the validity of the concept. An optimized injection flow rate eliminates most of the waves caused by the injection from the flow, and at least some of the remaining waves are believed to be caused by the discrete nature of the

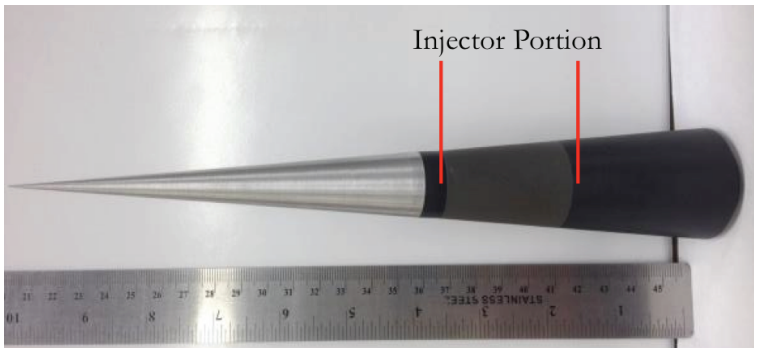

Figure 1. Conical porous injector assembly used in the current study. The injector portion was also used in the previous T5 studies.

grid, since the simulated injector is composed of a series of discrete holes, each one two cell widths wide, as opposed to the nearly flat surface associated with a porous injector. The result of the computation is shown in Figure 3. On a cone with a cylindrical section without injection, it is well-known that the boundary layer separates over the compression turn at the end of the cylindrical section. It will be investigated whether this occurs with injection.

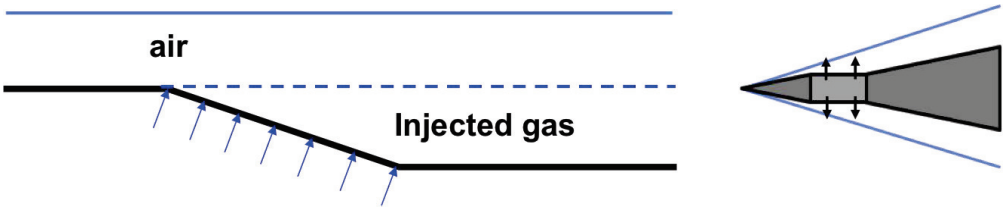

Figure 2. An illustration of the concept of a negative slope on the surface of the test article to compensate for the additional displacement thickness caused by injection. The model on the right shows the desired shock pattern, i.e. only the shock on the tip of the cone is present.

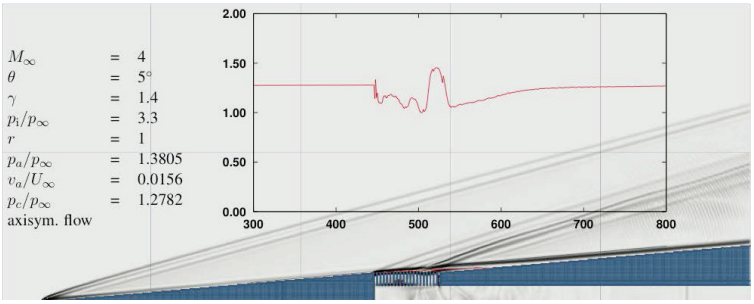

Figure 3. A numerical schlieren representation of an Euler computation of superosonic flow with injection, showing the minimization of waves caused by injection. The thin line above the cone shows the pressure distribution along the surface of the injector, which would be uniform if the injection had no effect on the surrounding flow.

II. Experimental Setup

Experiments for the current study were performed in the Mach 4 Ludwieg tube at Caltech. A perspective view of the facility is shown in Figure 4. The Ludwieg tube produces Mach 4 air flow with a freestream velocity of 670 m/s and a steady test time of 100 ms. The noise level is in the range of 0.4% in density.[10] A standard Z-type schlieren visualization setup is used to visualize the flow. A Phantom v710 high speed camera is used to record images, and two separate light sources are used. For sensitive, full-field images which clearly detect the shock system a Cree X-Lamp MC-E Cool White continuous white light LED is used, corresponding to a frame rate of 3000 frames per second with an exposure time of 30 μs. Images taken with this configuration cannot resolve small or transient structures in the flow, so a second light source is used in a separate set of experiments with a different frame rate to capture these. This light source is an

Osram SPL PL90-3 infrared laser diode with a wavelength of 905 nm. The beam is expanded to achieve a field of view surrounding the injector, and the diode is pulsed according to the frame rate of the camera, 100,000 fps with a pulse width of 40 ns using a PicoLAS LDP-V 50-100 V3 laser driver. This allows resolution of small-scale or transient structures in the flow that cannot be observed using the continuous light source, but with the sacrifice of some sensitivity. The pulsed diode technique in schlieren imaging is documented in Parziale et al.[11]

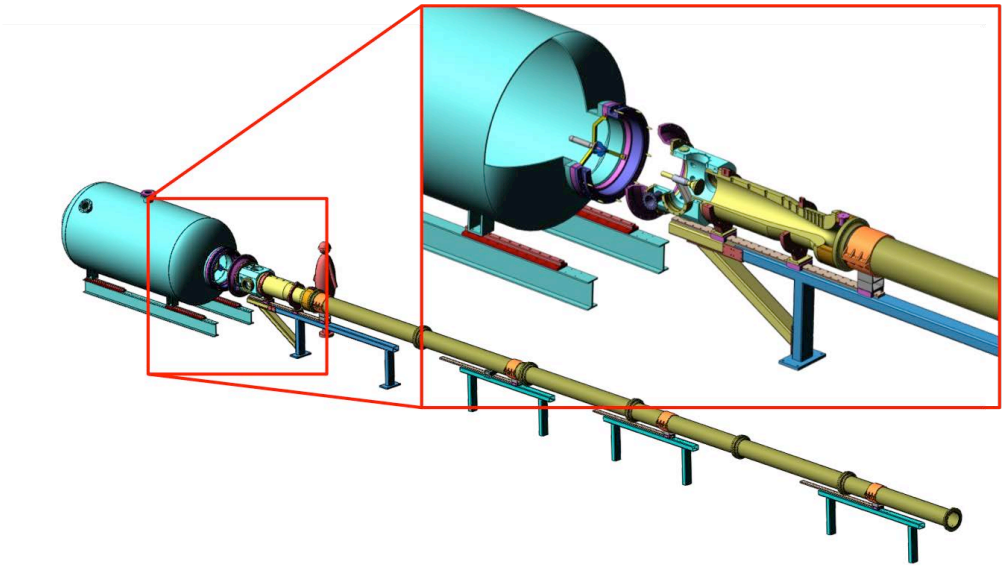

Figure 4. Solid model of the Caltech Ludwieg tube. The overall length of the facility is 23.5 m, the driver tube is 17 m long, and the nozzle exit diameter is 31.5 cm. $M_\infty = 4$, $T_\infty = 70$ **K,** $U_\infty = 670$ **m/s, and** $t_{\text{test}} = 100$ **ms**

In addition to the conical injector described previously, a cylindrical injector was also tested to investigate Fedorov's hypothesis of the potential benefit of shape changes on flow displacement. Both injectors are approximately 40 mm long with a diameter of 23 mm and are inserted between sections of a 5 degree half-angle cone. The beginning of the injector section is 127 mm from the tip of the cone. Both injectors are made from sintered 316L stainless steel with a mean pore size on the order of 1 μm. The permeability of each is calculated in Section III. The mass flow rate of injected gas is measured with a calibrated Sensirion EM1 mass flow meter and is presented as a parameter m, which is the injected mass flow rate normalized by the mass flow rate of the incoming laminar boundary layer based on δ_{99}. The injected gas flow at the surface is estimated to have a negligible streamwise velocity and a wall-normal velocity between 10 and 40 m/s depending on the mass flow rate. The incoming boundary layer profile is calculated using the Taylor-Maccoll solution for supersonic flow over a cone coupled with the similarity solution of Lees for a laminar compressible boundary layer on a cone. The boundary layer is observed with high-speed schlieren imaging to be laminar prior to the injector in all configurations. Calculated laminar velocity and density profiles are shown in Figure 5, these two are multiplied and integrated from zero to δ_{99} to calculate the mass flow rate. δ_{99} in this case is 0.75 mm and the mass flow rate of gas in the incoming boundary layer is calculated to be 0.80 g/s.

The unit Reynolds number is approximately 10^7/m, corresponding to a Reynolds number of 1.27×10^6 at the beginning of the injector. Under these conditions, stability calculations show that upstream of the injector only the "first mode" is unstable but eventually downstream of the injector location the growth rate of the "second mode" surpasses that of the first. The damping effect of the porous section has not been included in these calculations.

III. Porous Media Analysis

Before examining the results of the experiments it is worth while to analyze the flow through the porous injectors. A more complete discussion of the flow through the injectors can be found in a report by Schmidt.[12] Only the relevant results are reported here. The flow through an injector is assumed to be axisymmetric

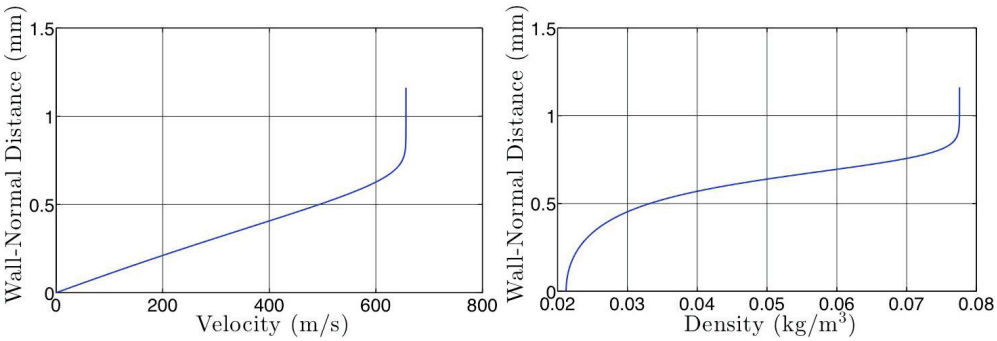

Figure 5. Results from a similarity solution computation for the laminar boundary layer profile at the beginning of the injector in the Ludwieg tube freestream.

and steady, and a relationship between the pressure inside the injector and the mass flow rate through the injector can be derived from the continuity and momentum equations. The continuity equation is

$$\frac{\mathrm{d}}{\mathrm{d}r}(\rho u) + \frac{\rho u}{r} = 0 \tag{1}$$

This reduces to

$$\rho u r = \text{constant} = \frac{\dot{m}}{2\pi L} \tag{2}$$

for a cylinder of length L. The momentum equation is a balance between the pressure difference across the injector and the drag inside the pores.

$$-\frac{\mathrm{d}p}{\mathrm{d}r} = \frac{\rho u^2 C_D}{\bar{d}} \tag{3}$$

Here C_D is a drag coefficient for the injector that is modeled using the Forchheimer equation and $\bar{d}$ is the mean particle diameter for the porous material, an unknown quantity that is related to the permeability κ. Using the Forchheimer equation for the drag coefficient and substituting the mass flow rate for velocity according to Equation 2, the following relation between pressure and mass flow rate is derived.

$$-\rho\frac{\mathrm{d}p}{\mathrm{d}r} = \frac{\dot{m}\mu}{2\pi L\kappa r} \tag{4}$$

Using the ideal gas law to express ρ as a function of p and T allows this equation to be integrated from the inside of the injector to the outside approximating the gas as isothermal through the injector, which is valid because the local Mach number remains small. This integration yields

$$p_i^2 - p_o^2 = \frac{\dot{m}\mu RT}{\pi L\kappa}\ln\left(\frac{r_o}{r_i}\right) \tag{5}$$

where subscripts i and o denote conditions at the inside and outside of the injector respectively. In the experiments, the pressure at the outside of the injector is the boundary-layer edge pressure for the cone, which can be computed according to the Taylor-Maccoll solution to be 1.73 kPa. The pressure required to drive an appreciable mass flow through the injector, as can be seen from Figures 6 and 7, is on the order of 100 kPa. Thus $p_o^2/p_i^2 << 1$ and Equation 5 can be approximated as

$$p_i^2 = \frac{\dot{m}\mu RT}{\pi L\kappa}\ln\left(\frac{r_o}{r_i}\right) \tag{6}$$

A set of experiments was performed to simultaneously measure the pressure inside the injector and the mass flow rate in order to confirm the validity of Equation 6 and determine the value of the permeability of each injector. A measurement unit fitted with a Kulite XT-190 piezoresistive pressure transducer was fitted to the front of the injector instead of the cone tip used in flow experiments, and the apparatus was placed inside the test section of the Ludwieg Tube at a partial vacuum of approximately 1.7 kPa to simulate the proper edge pressure that would occur during a flow experiment.

Figures 6 and 7 show the results of these experiments with air as the injected gas for each injector. The permeability κ is determined by linear least-squares by considering the relationship between pressure and the square root of the mass flow rate. It can be seen from Equation 6 that κ is the only unknown parameter, so it is determined by the fit that minimizes the total error. Uncertainty in κ is calculated by the quadrature sum of the uncertainty based on the 95% confidence interval of the curve fit and the propagation of uncertainty in pressure. The calculated values for permeability are typical for sintered metal.[13]

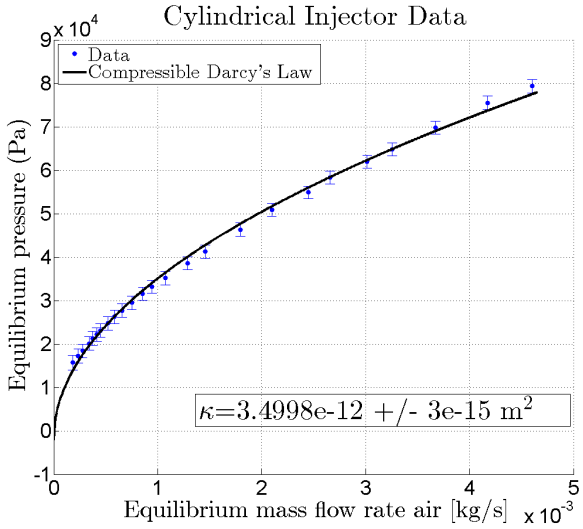

Figure 6. Pressure vs. mass flow rate data for air with the cylindrical injector fit with Equation 6 to determine permeability

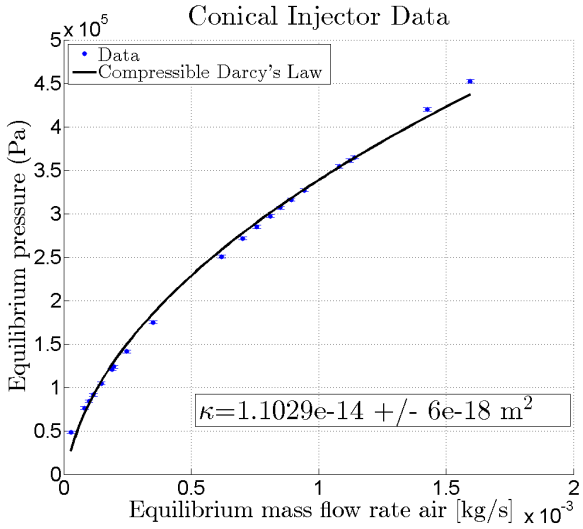

Figure 7. Pressure vs. mass flow rate data for air with the conical injector fit with Equation 6 to determine permeability

IV. Results and Discussion

Tests in supersonic flow are performed across a wide range of injection mass flow rates with both injectors. Although carbon dioxide would eventually be the injected gas in a boundary layer transition control experiment in hypervelocity flow, air was used as the injected gas in the current study. At room temperature, the temperature at which the gas is injected, carbon dioxide is not significantly vibrationally active, so injection of gases with such similar density is not expected to qualitatively alter the flow characteristics. This assumption is shown to be valid in a small set of experiments performed with carbon dioxide as the injected gas. Injecting air simplifies computational analysis of the flow since the mass transport equation decouples

from the Navier-Stokes equations. A brief computation is also performed to investigate the stability of the injection layer formed downstream of the injector.

IV.A. Experiment

Results from four tests with the conical injector are shown in Figure 8. The vertical lines on the cone model mark the location of the injector, and the parameter m again represents the normalized mass flow rate described in Section II. A stronger shock, relative to the shock at the cone tip, is visible in all three injection tests at the beginning of the injector due to the increased displacement thickness as predicted in Section I.B. The shock angle at the cone tip is determined to be 15° both by experiment and via the Taylor-Maccoll solution, which corresponds to a non-dimensional pressure jump of $\Delta p/p_1$ of 0.077. The shock angle at the beginning of injection is measured to be approximately 21° relative to the cone surface, corresponding to a pressure jump of $\Delta p/p_1$ of 1.016, or about 13 times stronger than the shock at the cone tip. The shock created by injection is curved, so it is difficult to precisely determine its angle at the surface of the cone, and the angle is 21° within experimental uncertainty for all injection mass flow rates studied. Besides appreciably disturbing the inviscid region of the flow, the oblique shock also creates a strong adverse pressure jump for the incoming boundary layer, potentially leading to separation or rapid transition to turbulence. A Prandtl-Meyer expansion can be seen following this shock, and a second oblique shock wave is visible at the end of the injector in tests with high mass flow rates. This wave system is what one would predict by modeling the additional displacement thickness over the injector as a convex bump on the surface of the cone.

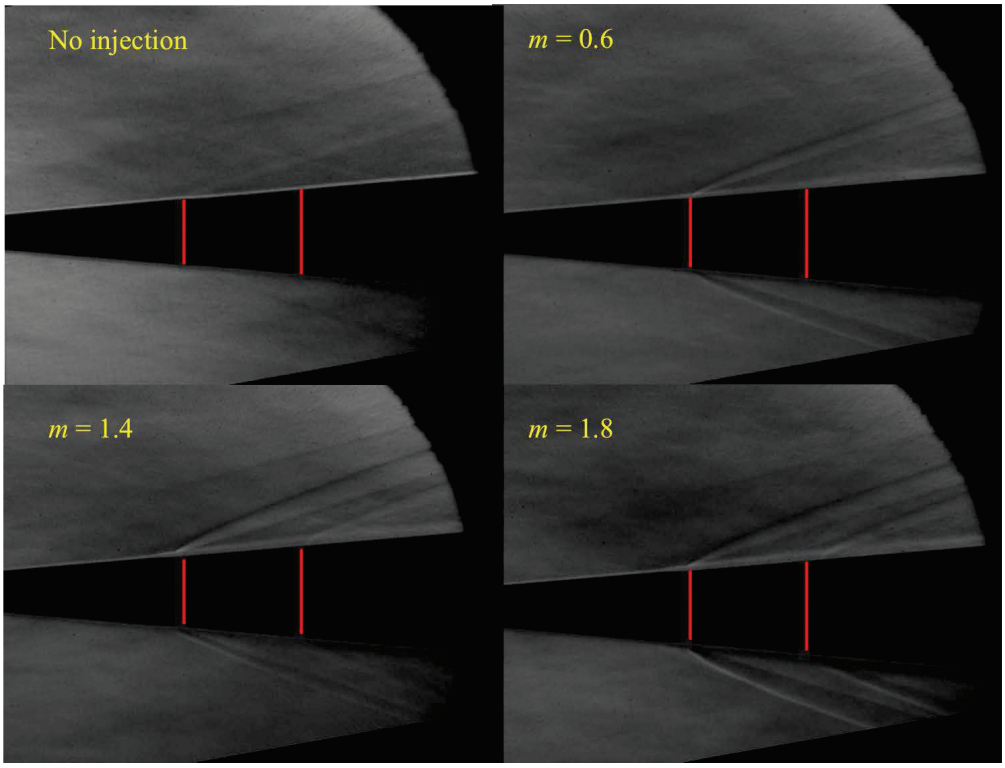

Figure 8. Results from conical injector experiments

Figure 9 shows the results from four representative tests with the cylindrical injector. Three regimes are possible in this configuration. In cases with high mass flow rates, represented by $m = 1.0$ and $m = 1.5$, an oblique shock is still formed at the beginning of the injector as the additional displacement thickness from injection overcompensates for the negative slope of the injector itself. If the mass flow rate is sufficiently small, such as $m = 0.3$, the injection is not large enough to compensate for the shape change of the injector resulting in a weak Prandtl-Meyer expansion at the beginning of the injector. However, at a normalized mass flow rate of approximately $m = 0.5$ the slope from the increasing displacement thickness exactly matches the slope of the cone and no visible waves are observed to propagate into the free stream. The mean flow is therefore closely matched to flow past a cone with no injection and no changes to its geometry. These

results validate the hypothesis of Fedorov and demonstrate that it is possible to inject gas in the boundary layer around a body with a minimal impact on the exterior supersonic flow.

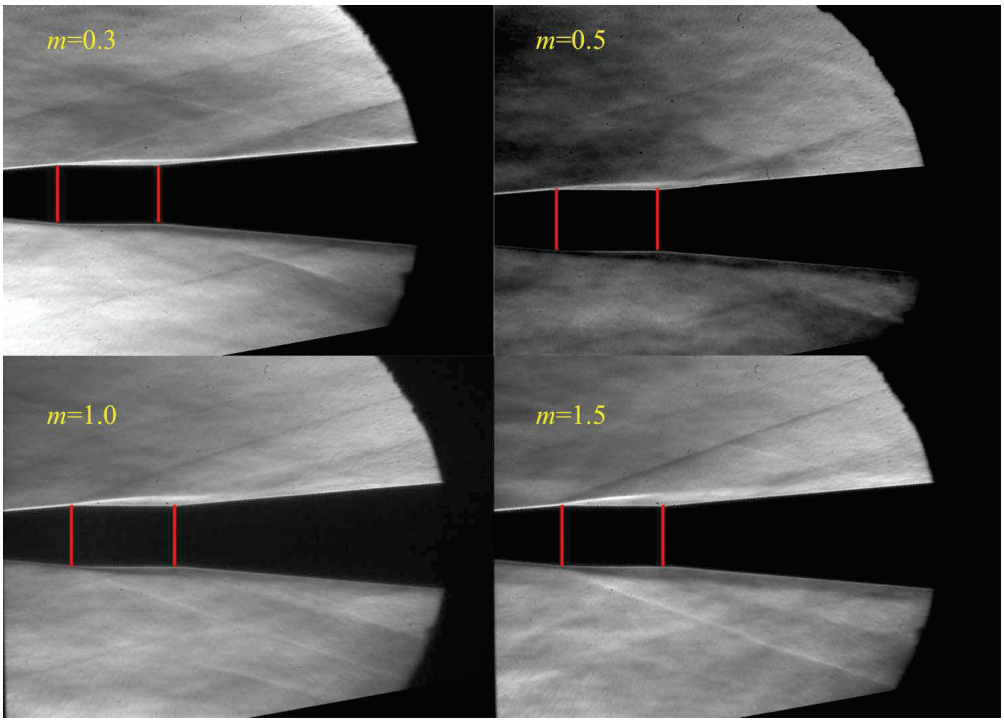

Figure 9. Results from cylindrical injector experiments

For the specific application of influencing boundary layer transition, the key issue is the effect of injection on boundary layer stability: does the boundary layer transition rapidly from laminar to turbulent flow or does it remain laminar downstream? Previous work by Pappas and others reveal that injection on a cone causes transition to occur earlier than with no injection in cold supersonic flow with lighter injected gas having a more pronounced effect.[14] Shaping of the injector was not considered so any effect a cylindrical injector has versus a conical injector is not discussed.

The long exposure time images in Figure 9 do not allow stability to be investigated, but it is possible using images taken with the 40 ns pulsed laser. Figure 10 shows an image taken with the laser source revealing regular turbulent structures forming downstream of injection. The structures appear to be very similar to those noted by Pappas and Okuno[14] but the nature of the instability is unclear. The laser source also reveals that with injection the boundary layer does not separate over the compression turn at the aft end of the injector. It is difficult to determine in experiments if the boundary layer separates without injection, but the computations described in Section IV.B reveal that it does.

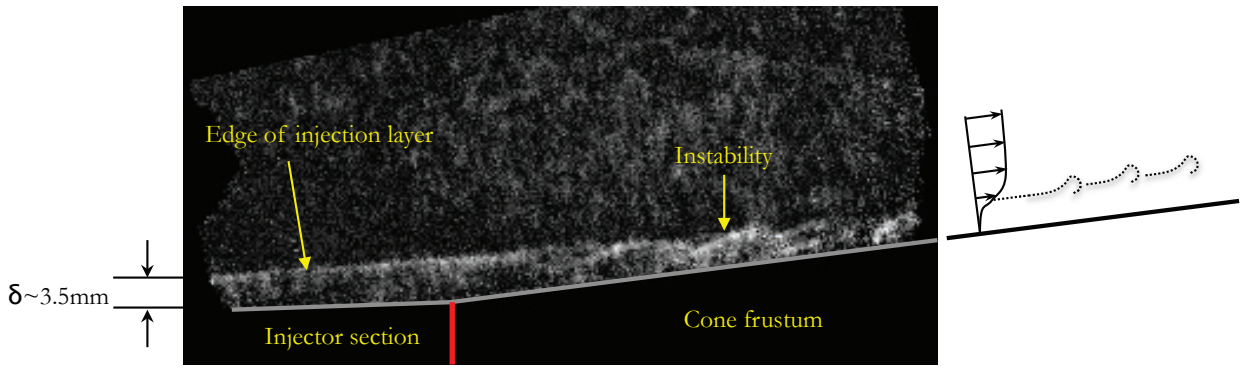

Figure 10. Schlieren image from a test with 40 ns exposure with $m = 0.6$. The rear of the injector is marked with a vertical line. A sketch on the right shows the velocity profile and the resulting production of vorticity. The instability of the injection layer is clearly visible downstream of the injector.

Schneider associates the injection layer instability with a second mode instability as would be present in a boundary layer, in other words, the injection layer instability is caused by trapped acoustic waves. This may be the case, but the injection layer transition might instead be caused by a Kelvin-Helmholtz instability at the interface of the low-speed injected stream and the high speed flow around the cone. Alternatively both effects could be present and the amount of injection may change their relative strengths. Further experimental work is required in order to make quantitative measurements of the instability and make more definitive statements about its nature. Some numerical stability computations are presented in Section IV.B and a more complete numerical analysis of this flow is performed in the companion paper by Fedorov.

IV.B. Stability Calculations

A numerical stability analysis was performed as a preliminary effort to quantitatively examine the stability characteristics of the injection layer formed downstream of injection. Injection layer and boundary layer profiles are found from a computation using experimental conditions for the cylindrical injector at the tuned condition where waves are minimized. Computations were performed in OpenFOAM using the rhoCentralFoam solver, a density-based compressible flow solver for the Navier-Stokes equations based on the central-upwind schemes of Kurganov and Tadmor. The original mesh was an axisymmetric 605-by-200-cell grid with grading to improve resolution close to the cone surface, especially near the injector. A convergence study was performed on a 1210-by-400-cell grid, which revealed convergence. Results in this section are from the fine grid for higher resolution in the boundary layer.

Freestream conditions are chosen to match those in the Ludwieg Tube. The freestream velocity is 670 m/s, the pressure is 1335 Pa, and the temperature is 70 K. The injector section is modeled by a wall boundary condition of uniform normal velocity and pressure at ambient room temperature. The other walls are assumed to be adiabatic. The tuned condition occurs at an injection velocity of 10 m/s, a pressure along the surface of the injector of 1137 Pa, and a temperature of 295 K. The pressure and velocity can be chosen independently in the boundary condition, but the pressure matches that of the flow immediately outside of the injector within 1-2 cells and the velocity corrects itself accordingly. These values correspond to a mass flow rate of 0.39 g/s, which gives a value of m of 0.49, matching the tuned injection rate for the experiments. Both the freestream and injected gases are air, and Sutherland's formula is used to calculate viscosity. The simulation is run for 1 ms in real time, which results in 2.5 flow lengths with a maximum allowable Courant number of 0.6. The computation is observed to converge in this time.

Figure 11 shows a numerical schlieren result for the computation. Note its resemblance to Figure 9. Figure 12 shows the evolution of the boundary and injection layer profiles over the length of the cone. These were used to analyze stability. The number of points in the boundary layer ranges from 90 just before the injector to 140 far downstream of the injector, which are sufficient for differentiation.

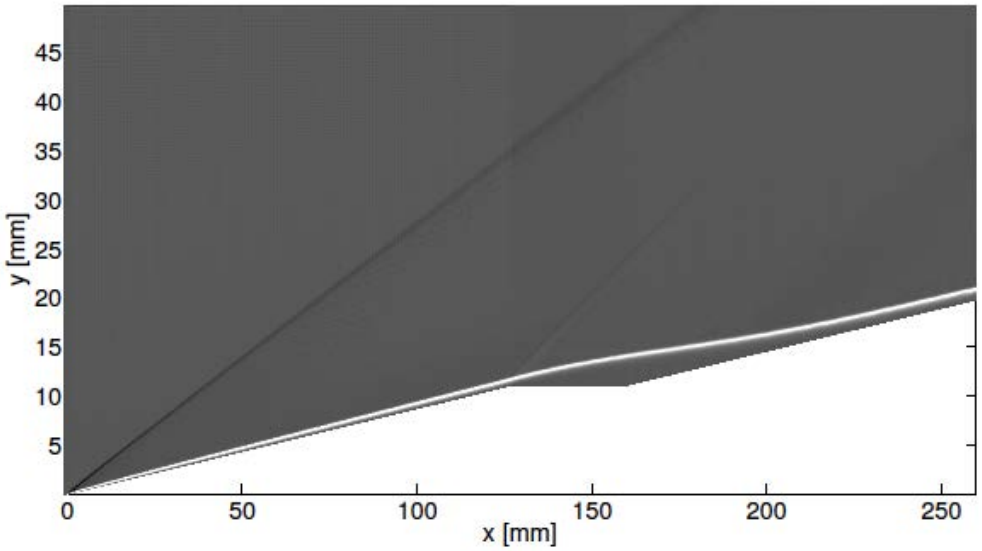

Figure 11. Numerical schlieren for the tuned injection rate from the OpenFOAM computation

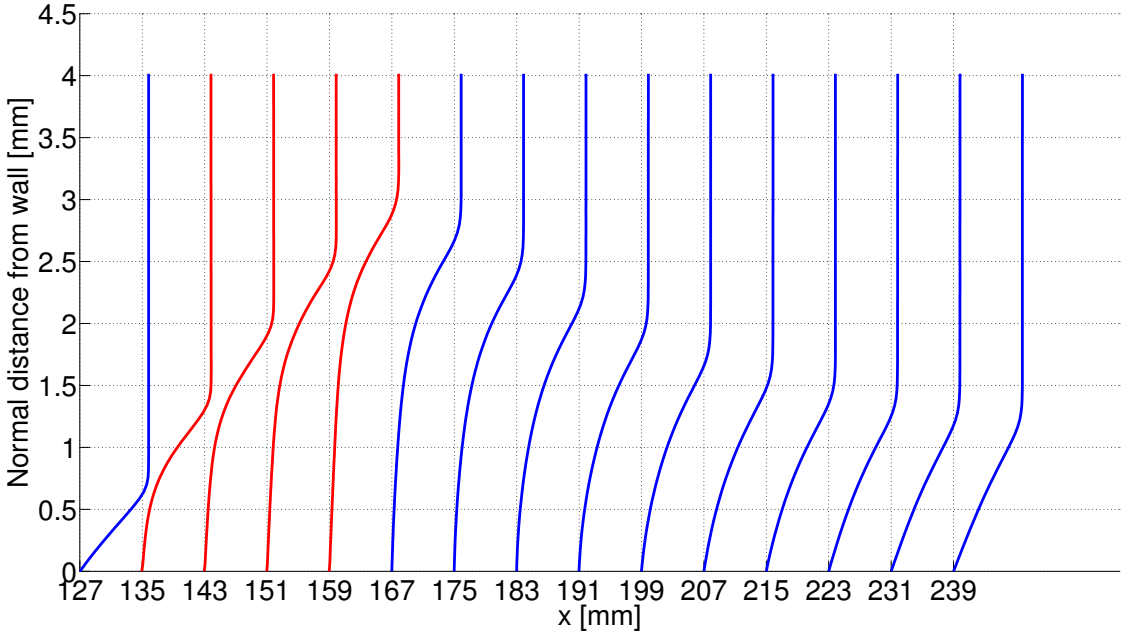

Figure 12. Velocity profiles near the wall along the length of the cone with the cylindrical injector for $m = 0.5$. Spacing between profiles is 8 mm. Red profiles are over the injector section.

At each streamwise location x, a locally parallel, spatial stability calculation is conducted using the shooting method developed by Mack.[15] Perturbations of the form $\mathbf{q}(y)\exp(i\alpha x + i\beta z - i\omega t)$ are substituted into the linearized Navier-Stokes equations, where $\mathbf{q}$ is the vector of physical variables $(\hat{u}, \hat{v}, \hat{w}, \hat{p}, \hat{\theta})^T$ and α and β are the streamwise and spanwise wavenumbers. The linearized Navier-Stokes equations are then cast in the form:

$$\frac{\partial \mathbf{q}}{\partial y} = \mathbf{A}\mathbf{q} \tag{7}$$

where $\mathbf{A}$ is an 8×8 matrix whose coefficients are given by Malik.[16] This system of equations is solved starting in the freestream where the asymptotic behavior is known (see Mack[15]), and the disturbances are required to be asymptotically decayed as $y \to \infty$; on this basis four of the fundamental solutions of Eq. 7 are rejected and four are retained. The four acceptable (decaying) fundamental solutions are then integrated towards the wall using a fourth order Runge-Kutta routine. Gram-Schmidt orthonormalization is employed intermittently as this integration proceeds to control parasitic growth of numerical errors.[17–19] Linear combinations of the four decaying solutions of Eq. 7 are taken at the wall to satisfy the homogeneous velocity boundary conditions $\hat{u} = \hat{v} = \hat{w} = 0$ and the normalization condition $\hat{p} = 1$, while the remaining homogeneous boundary condition on the temperature fluctuation, $\hat{\theta} = 0$, is satisfied when an eigenvalue α has been found. The complex eigenvalue search is conducted using the secant method with a convergence tolerance of 10^{-5}. The code used to perform the stability analysis has been validated by reproducing the results of several other researchers for flat-plate boundary layers under hypersonic, perfect gas conditions.[4,16,20,21]

Locally parallel stability analyses are conducted independently at each streamwise location x. Velocity and temperature profiles are generated by projecting the results of the OpenFOAM simulations onto wall-normal planes, and the data are interpolated onto a finer grid (1000 points) for the stability calculations in order to capture the finer features of the disturbances. The analysis is locally parallel, meaning that streamwise gradients in the mean flow are ignored, as is the wallnormal velocity. The neglect of the wallnormal velocity is reasonable since the injection velocity (10 m/s) is only 1.5% of the freestream velocity. Likewise, the wallnormal component of velocity in the freestream above the injector (caused by the change in slope of the wall) is only 8.7% of the tangential velocity component. However, the parallel flow approximation is questionable in the injection region since the mean flow varies strongly in the streamwise direction. Although these factors are likely to quantitatively affect the disturbance growth rates, the present study is still expected to furnish the qualitative influences of injection on the stability of the boundary layer.

Examples of calculated spatial growth rates at eight different streamwise locations are shown in Figs. 13-

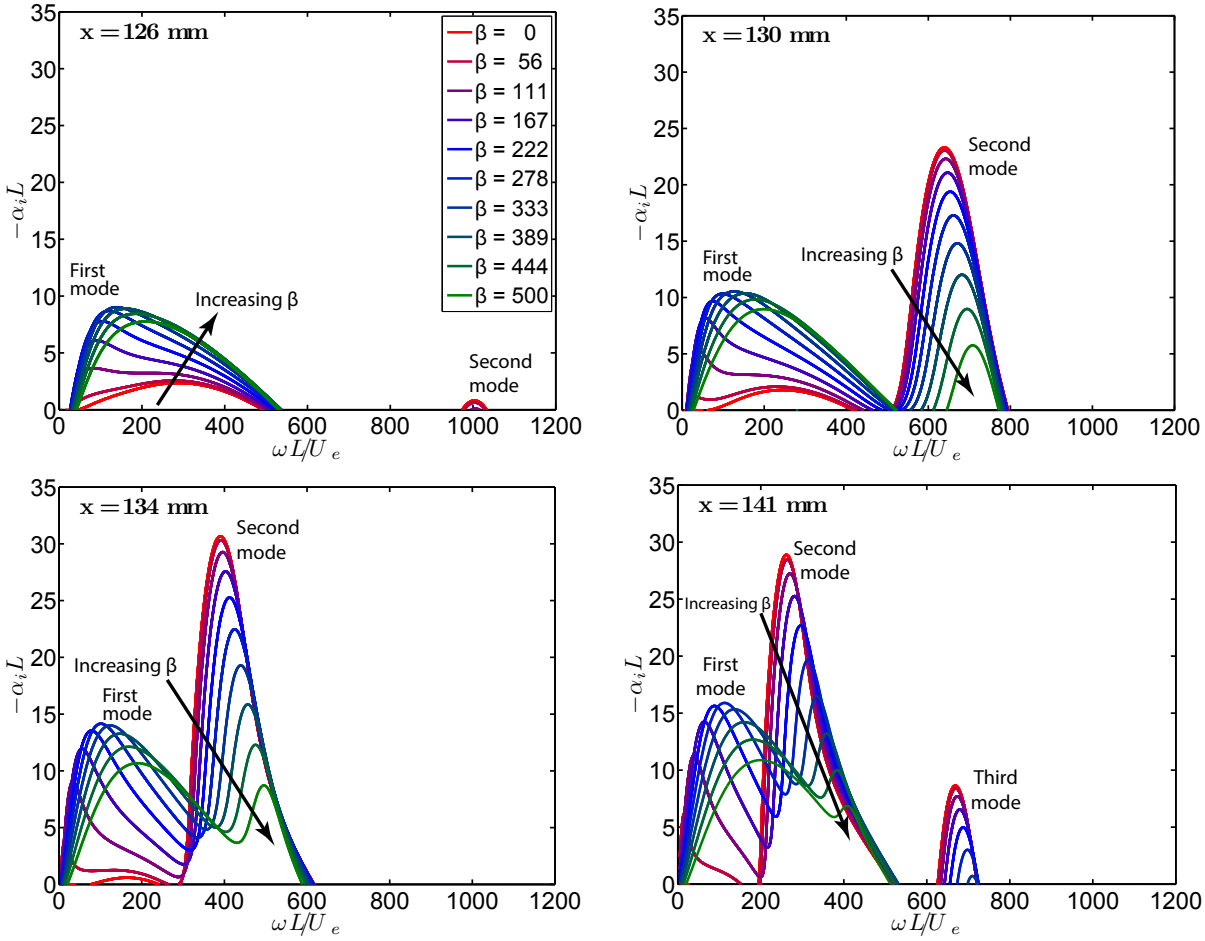

Figure 13. Three dimensional spatial growth rates at four stations along the injector. Each line represents a different spanwise wavenumber, β. The injector extends from $x = 127$ mm to $x = 160$ mm.

14. Each plot contains multiple lines corresponding to different values of the spanwise wavenumber β, which are indicated by the line colors and also by an arrow in the direction of increasing β. The injector begins at $x = 127$ mm and ends at $x = 160$ mm. Upstream of the injector ($x = 126$ mm), the stability characteristics are the same as those for flow over a sharp cone or flat plate. The first mode is slightly unstable with a three dimensional perturbation having the largest growth rate, and the second mode is nearly neutrally stable. At $x = 130$ mm, slightly past the front of the injector, the second mode is destabilized significantly while the first mode is only slightly affected. There is also a large reduction in the frequency at which second mode is maximized, which is a result of the increased thickness of the injection layer. Further downstream at $x = 134$ mm, the growth rate of the second mode continues to increase and its frequency continues to decrease. The first mode is also noticeably destabilized, but not to the same extent as the second mode. At $x = 141$ mm, about midway along the injector, the third mode also becomes unstable and both the second and third modes continue to shift towards lower frequencies.

Near the end of the injector, $x = 159$ mm, the third mode continues to destabilize while the growth rate of the second mode decreases slightly. Beyond the injector ($x = 182$ mm) the second and third modes begin to stabilize and move back to higher frequencies as the injection layer becomes thinner, and as the end of the cone is approached the stability characteristics relax back towards those of an adiabatic cone or plate. However, even at the largest downstream distance of $x = 250$ mm the injection layer has not quite relaxed completely to a self-similar boundary layer profile.

Similar behavior is reported in the companion paper by A. Fedorov, but there are some differences because they are modeling a high enthalpy boundary layer. In their case, the wall temperature is extremely cold relative to the freestream temperature, which is well-known to de-stabilize the acoustic modes and stabilize the first mode.[4] Additionally, most of their cases involve much greater normalized injection rates than we

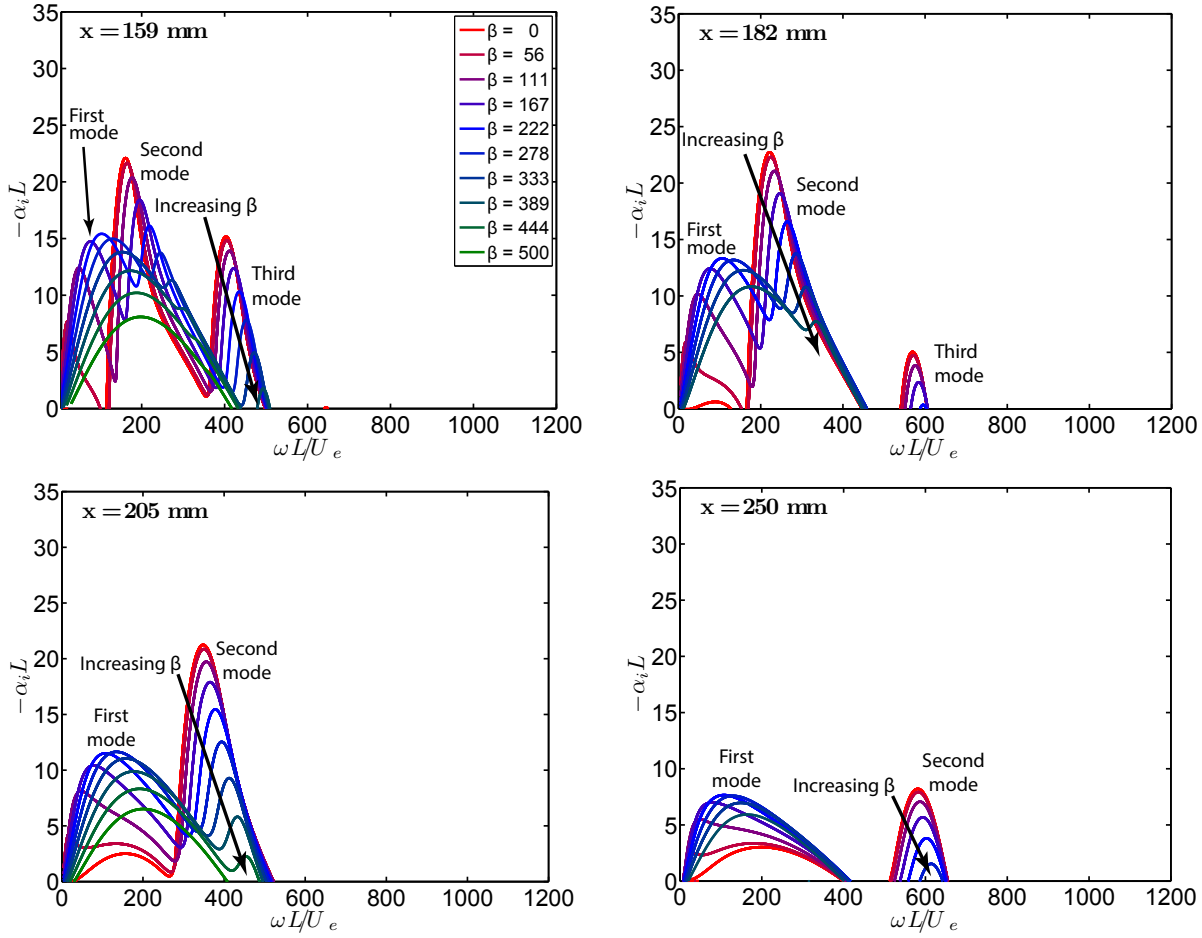

Figure 14. Three dimensional spatial growth rates at four stations along the injector. Each line represents a different spanwise wavenumber, β. The injector extends from $x = 127$ mm to $x = 160$ mm.

consider here, which strengthens the inflection point in the velocity profile and enhances the dead zone above the injector. Because of these differences, they see six unstable acoustic modes rather than two and they see no first mode instability.

It is noteworthy that in the injection region the unstable modes retain their identities as "first mode" or "higher mode" disturbances and are easily identified by their phase speed and the number of peaks in the pressure eigenfunction. That is, qualitatively the injection layer that develops behind the injector behaves similarly to an ordinary boundary layer, though the modes are destabilized by the increased injection layer thickness. This resemblance between high Mach number boundary layers and compressible shear layers was recognized by Mack,[4] who pointed out that "the instability characteristics of flat-plate boundary layers above $M_1 = 3$ are more like those of a free shear layer than of a low-speed zero pressure-gradient boundary layer." The stability characteristics of the injection layer are in many ways similar to those observed for high Mach numbers (on the order of 10 or higher), where the boundary layer is thickened by viscous dissipation and the destabilization of multiple acoustic modes is common. Apparently the stability of the acoustic modes is sensitive mainly to the location of the relative sonic line and is less sensitive to the actual distributions of velocity and temperature.

IV.C. Alternative Configurations

Although it is possible to minimize waves formed by injection by using a cylindrical injector instead of a conical one, the injection layer is still unstable by acoustic instabilities. The instability rapidly leads to a transition to turbulence downstream of the injector, negating any potentially stabilizing effects from a vibrationally active gas. Two alternative configurations have been considered in an attempt to create a more stable injection layer.

The first relies on the fact that porous coatings have a stabilizing effect on hypervelocity boundary layers.[9] A non-injecting porous coating covering the wall of the cone immediately downstream of the injector could absorb acoustic energy in the injection layer, increasing stability and potentially preventing transition, thus allowing the injected gas to further absorb destabilizing acoustic radiation. This idea is investigated more thoroughly in computations by Fedorov in the companion paper. Stabilizing effects of the porous media used for injectors was not considered in this study.

The second configuration is to inject the gas tangentially to the surface of the cone in order to create a more stable velocity profile than those shown in Figure 12. The velocity profiles created by normal injection have an inflection point, which is typically unstable for a boundary layer. The inflection point is caused by the injection of fluid with very low streamwise momemtum close to the wall which comes into contact with the high speed stream at the edge of the boundary layer, which could be thought of as a wall-bounded shear layer instead of a boundary layer with an inflection point. If gas could be injected tangentially with comparable velocity to the freestream, perhaps a stable velocity profile could be created. Figure 15 illustrates the idea. Tangential injection would create a wake-like velocity profile instead of one akin to a shear layer.

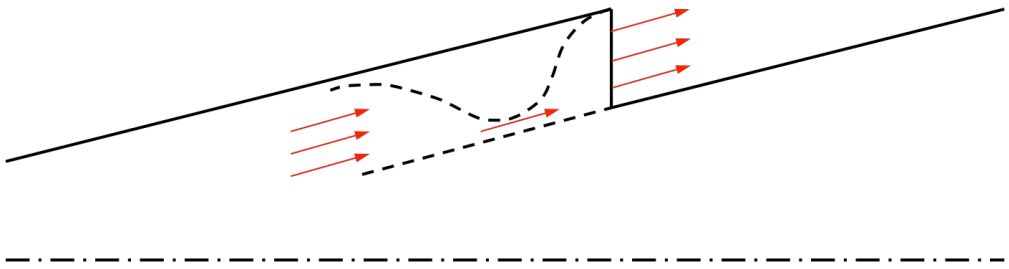

Figure 15. Schematic for a tangential injection scheme.

There are issues with accelerating the injected gas to sufficient velocity to prevent creating a shear layer-like velocity profile. The width of the slot through which the injected gas exits should be on the order of the boundary layer thickness, about 1 mm, to produce the desired effect. A converging-diverging profile must be created leading to the exit in order to accelerate the gas, and the carbon dioxide cannot be expanded from room temperature to the desired velocity without undergoing a phase change and requiring a very narrow throat, on the order of tens of microns. It is found that if the gas is heated to roughly 500 K the issues of encountering a phase change and requiring an overly narrow throat are resolved.

In order to calculate the flow through the injector channel, a quasi-1D approach is taken which considers friction and the changing area. A converging-diverging profile is generated using two cubic polynomials with the slopes and positions of the entrance, throat, and exit specified. The goal of the present analysis is only to understand the required reservoir conditions to produce high-velocity flow of carbon dioxide through a narrow exit. Figure 16 shows the thickness of the injector. The bottom of the profile is simply the edge of a cone with a beginning radius of 2 cm and a half-angle of 5°. The injector is 10 cm long. The initial width of the injector channel is 1 mm with an exit width of 0.8 mm and a throat width of 0.35 mm. The throat is located at 80% of the length of the injector in order to prevent substantial deceleration of the flow due to friction. These parameters were chosen to correspond to a model that could potentially be tested in the $M = 4$ Ludwieg Tube at Caltech. The objective exit velocity and pressure are approximately 600 m/s and 1.7 kPa respectively to match typical boundary layer edge conditions on a cone model, and the reservoir temperature is specified to be 500 K to avoid the issues described above. The profile analyzed is not optimized in any way and may be unrealistic, but it serves to demonstrate the importance of considering the effects of friction, particularly in decelerating the flow in the diverging section.

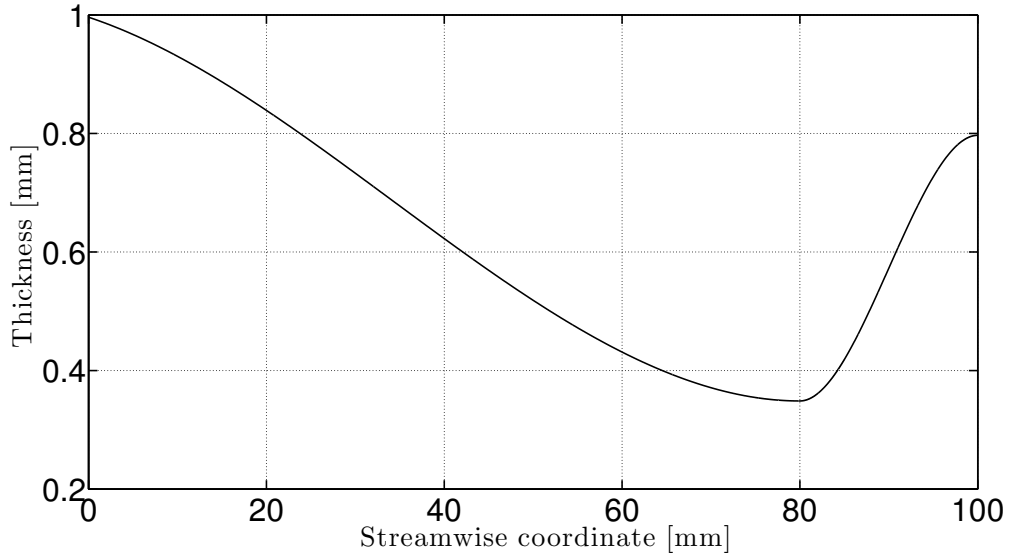

Figure 16. Thickness as a function of streamwise variable of modeled tangential injector with dimensions in millimeters.

The area as a function of streamwise variable x can be calculated from this profile and some geometrical considerations. The differential equation to be solved is derived in Shapiro.[22] It is an ODE for the Mach number squared as a function of the streamwise variable and is a linear combination of terms for area change and friction. In the following equation, C_f is the Darcy friction factor and D_H is the hydraulic diameter, four times the area divided by the wetted perimeter.

$$\frac{1}{M^2}\frac{d(M^2)}{dx} = -\frac{2\left(1+\frac{\gamma-1}{2}M^2\right)}{1-M^2}\frac{1}{A}\frac{dA}{dx} + \frac{\gamma M^2\left(1+\frac{\gamma-1}{2}M^2\right)}{1-M^2}\frac{4C_f}{D_H} \tag{8}$$

Note that the frictional term always drives the flow towards sonic conditions, and its strength grows like the Mach number squared for large Mach numbers while the area term becomes independent of Mach number and only depends on the rate of change of area for large Mach numbers. Therefore to produce a high exit Mach number wth a narrow nozzle like the one analyzed here, the diverging section must be short with a high rate of change in area in order to prevent the flow from quickly decelerating back to sonic conditions due to friction. This sort of a design is not typical for supersonic nozzles because typically a design goal is that the flow is parallel and uniform at the exit. A tradeoff exists in designing nozzles with narrow profiles where the Reynolds number is not large so that viscous effects are important, and one should not expect such a narrow nozzle to resemble a typical supersonic nozzle for inviscid flow. Two-dimensional viscous computations will need to be performed in order to properly optimize a design for the injector profile. Again, the objective of this analysis is only to demonstrate the issues associated with generating high-speed flow through a narrow injector profile and the injector profile presented here is in no way considered to be realistic.

The injector profile is divided into 25,000 points with the majority of points near the throat. The mass

flow rate is specified to be 5 g/s, respectively, and the friction factor is assumed to be uniformly 0.0025 throughout the injector. A 4th-order Adams-Bashforth-Moulton (ABM-4) predictor-corrector method is used to integrate Equation 8 from the beginning of the injector to the end with a 4th-order Runge-Kutta method used to start the ABM-4 integrator. Equation 8 is singular at $M^2 = 1$, but this is a removable singularity and due to the discrete nature of the computational grid the equation can be integrated through the singularity by carefully specifying the entrance Mach number and briefly switching from ABM-4 to the explicit Runge-Kutta method near the throat. There is still a slight discontinuity in the rates of change of certain flow properties near the throat with this method, but it serves the purposes of this analysis.

The algorithm was first tested with a friction factor of 0, which is simply an isentropic calculation. The results from this computation can be compared with one-dimensional isentropic flow relations. The relative error in area ratio as a function of Mach number is one way to assess the accuracy of the computation. It increases near the throat, but is less than 0.01% throughout the injector.

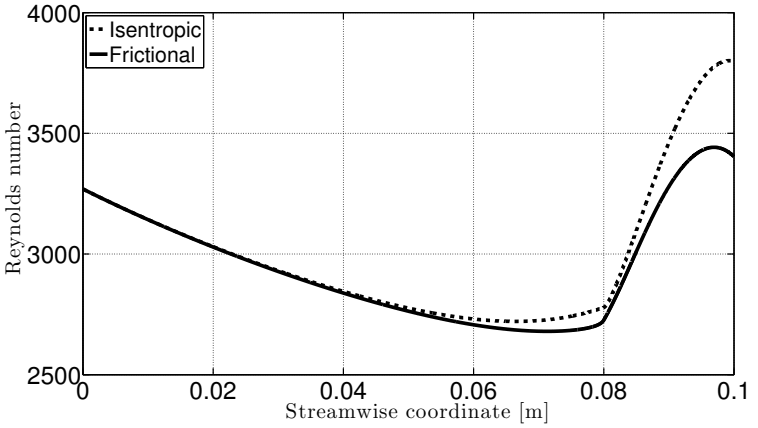

Figure 17. Reynolds number through the injector computed isentropically and with friction based on hydraulic diameter.

Figure 17 shows the Reyonlds number computed throughout the tangential injector. The maximum Reynolds number in the frictional case is less than 3500, meaning that viscous effects are essential to include. Again, a viscous, two-dimensional computation should be performed to properly calculate the flow through the injector.

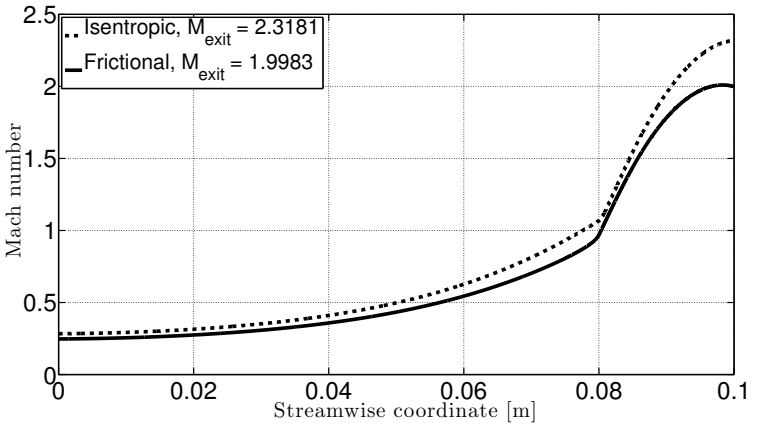

Figure 18. Mach number through the injector computed isentropically and with friction. Friction causes a slight reduction in exit Mach number.

Figures 18-21 show the Mach number, pressure, temperature, and velocity inside the injector as a function of streamwise coordinate x for both an isentropic and a frictional computation. Friction is found to change the exit conditions by 10-15%, but most importantly demonstrates a decrease in velocity with increasing area near the exit as predicted by Equation 8. This demonstrates the importance in a narrow nozzle of having a short diverging section with a high rate of expansion in order to achieve a high exit velocity. The computation shows the feasibility of such an injector, as the required reservoir condition of 25 kPa and 500 K can be attained without much difficulty. Further analysis of the multi-dimensional viscous flow is needed

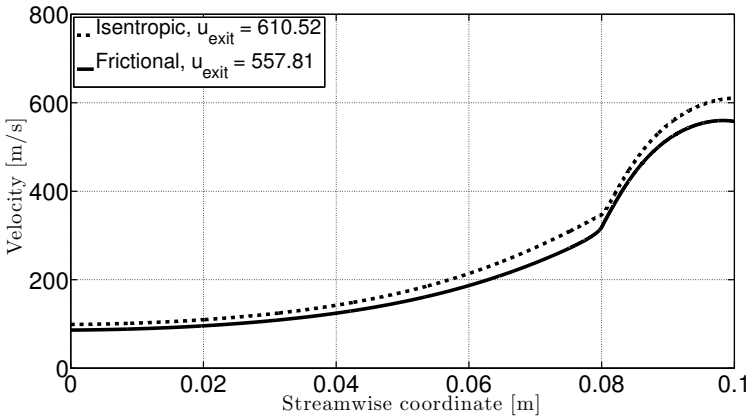

Figure 19. Velocity computed through the injector. Note that the velocity begins to decrease near the exit due to frictional effects.

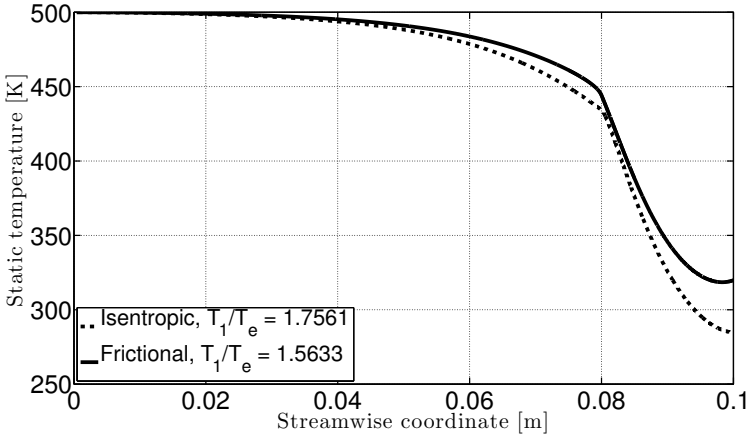

Figure 20. Temperature computed as a function of streamwise variable through the injector. The effect of friction is to prevent reduction in temperature due to expansion.

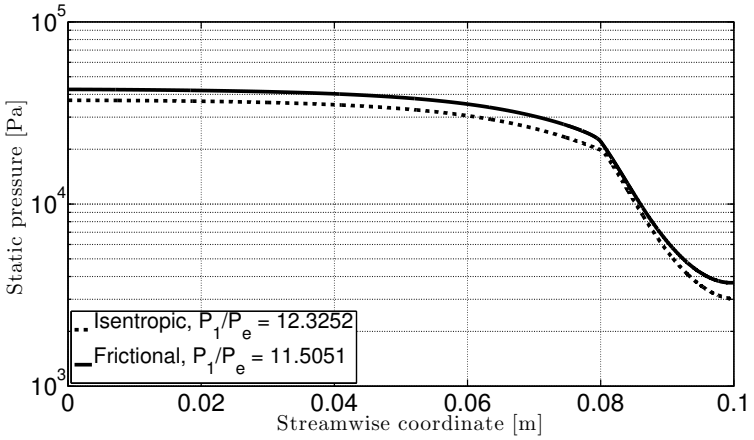

Figure 21. Pressure computed as a function of streamwise variable through the injector.

to create a realistic design. The stability characteristics of high-speed tangential injection have not been examined but clearly need to be explored as part of any future development.

V. Conclusions and Future Work

An experimental study was performed to examine the effects of injecting gas into the boundary layer on a slender body in supersonic flow. Of particular interest is the stability of the injection layer formed downstream of injection and whether through shaping the injector a stable flow could be created that would allow a vibrationally active gas such as carbon dioxide to stabilize a hypervelocity boundary layer. Injector shaping helps to minimize waves formed by injection, but injection still creates an unstable layer near the wall of the body. Other possible configurations could possibly stabilize the injection layer, although these ideas have not been thoroughly tested.

The nature of the instability created by injection is of interest as no quantitative measurements of the instability exist.[14] An experimental campaign to make such quantitative measurements is currently underway. Applications for injection in delaying boundary layer transition are limited because of the instability, but because turbulence is desired in scramjet inlets injection in supersonic flow remains a highly relevant research topic.

Acknowledgments

The authors would like to thank Dr. Nicholaus Parziale and Mr. Bahram Valiferdowsi for guidance and assistance in the laboratory. The authors would additionally like to acknowledge Dr. Joseph Jewell, Dr. Ivett Leyva, and Dr. Ross Wagnild for previous work done on this topic. Finally, the authors thank Dr. Alexander Fedorov for the concept of using a negative slope on the cone surface to compensate for injection. Without this key idea this work would not have been performed. This work was sponsored in part by AFOSR and NASA through the National Center for Hypersonic Research in Laminar-Turbulent Transition and also by AFOSR award number FA9550-10-1-0491. The views expressed herein are those of the authors and should not be interpreted as necessarily representing the official policies or endorsements, either expressed or implied, of AFOSR or the U.S. Government.

References

[1]J. E. Barth, V. Wheatley, and M. K. Smart. Hypersonic turbulent boundary-layer fuel injection and combustion: Skin-friction reduction mechanisms. *AIAA Journal*, 51(9), September 2013.

[2]S. A. Berry, A. H. Auslender, A. D. Dilley, and J. F. Calleja. Hypersonic boundary-layer trip development for hyper-x. *Journal of Spacecraft and Rockets*, 38(6), November-December 2001.

[3]J. S. Jewell, I. A. Leyva, N. J. Parziale, and J. E. Shepherd. Effect of gas injection on transition in hypervelocity boundary layers. In *28th International Symposium on Shock Waves*. Springer Berlin Heidelberg, 2012.

[4]L. M. Mack. Boundary-layer linear stability theory. Technical Report AD-P004 046, Jet Propulsion Laboratory and California Institute of Technology, Pasadena, CA (USA), 1984.

[5]A. V. Fedorov. Transition and stability of high-speed boundary layers. *Annual review of fluid mechanics*, 43:79–95, 2011.

[6]K. Fujii and H. G. Hornung. A procedure to estimate the absorption rate of sound propagating through high temperature gas. Technical Report FM 2001.004, California Institute of Technology, Pasadena, CA (USA), 2001.

[7]R. M. Wagnild, G. V. Candler, I. A. Leyva, J. S. Jewell, and H. G. Hornung. Carbon dioxide injection for hypervelocity boundary layer stability. Technical Report AFRL-RZ-ED-TP-2009-439, Air Force Research Laboratory, Edwards AFB, CA (USA), 2009.

[8]I. A. Leyva, J. S. Jewell, S. Laurence, H. G. Hornung, and J. E. Shepherd. On the impact of injection schemes on transition in hypersonic boundary layers. In *16th AIAA International Space Planes and Hypersonic Systems and Technologies Conference*, number 2009-7204. AIAA, 2009.

[9]A. V. Fedorov, N. D. Malmuth, A. Rasheed, and H. G. Hornung. Stabilization of hypersonic boundary layers by porous coatings. *AIAA Journal*, 39(4):605–610, 2001.

[10]Dirk Heitmann. Transition and stability measurements in hypervelocity flow around capsule-shaped re-entry bodies. Report on Results of the DAAD project, 2013.

[11]N. J. Parziale, Jason Damazo, B. E. Schmidt, and Patrick Wang. In preparation, 2014.

[12]B. E. Schmidt. Compressible flow through porous media with application to injection. Internal Report FM 2014.001, California Institute of Technology, 2014.

[13]T. H. K. Frederking, W. A. Hepler, S. W. K. Yuan, and W. F. Feng. Determination of the darcy permeability of porous media including sintered metal plugs. *Advances in Cryogenic Engineering*, pages 505–515, 1986.

[14]S. P. Schneider. Hypersonic boundary-layer transition with ablation and blowing. *Journal of Spacecraft and Rockets*, 47(2), March-April 2010.

[15]Leslie M. Mack. Computations of the stability of the laminar compressible boundary layer. In B. Alder, S. Fernback, and M. Rotenberg, editors, *Methods in Computational Physics*, volume 4, pages 247–299. Academic Press, New York, 1965.

[16]M. R. Malik. Numerical methods for hypersonic boundary layers. *Journal of Computational Physics*, 86:376–413, 1990.

[17]S.D. Conte. The numerical solution of linear boundary value problems. *SIAM Review*, 8(3):309–321, July 1966.

[18]V.K. Garg. Improved shooting techniques for linear boundary value problems. *Computer Methods in Applied Mechanics and Engineering*, 22(1):87–99, April 1980.

[19]A. Davey. An automatic orthonormalization method for solving stiff boundary-value problems. *Journal of Computational Physics*, 51(2):343–356, August 1983.

[20]A. Fedorov and A. Tumin. High-speed boundary-layer instability: Old terminology and a new framework. *AIAA Journal*, 49(8):1647–1657, August 2011.

[21]Yanbao Ma and Xaiolin Zhong. Receptivity of a supersonic boundary layer over a flat plate. part 1. wave structures and interactions. *Journal of Fluid Mechanics*, 488:31–78, 2003.

[22]A. H. Shapiro. *The Dynamics and Thermodynamics of Compressible Fluid Flow*, volume 1. Wiley, 1953.